RF-Photonic Spatial-Spectral Channelizing Receiver

William Beardell, *Student Member, IEEE*, Benjamin Mazur, Conor Ryan, Garrett Schneider, Janusz Murakowski, and Dennis Prather, *Fellow, IEEE*

***Abstract*—As mobile beam-bandwidth-product requirements accelerate, millimeter-wave (mmW) bands have been opened to telecommunications networks to enable wider channel bandwidths, while Massive Multiple-Input Multiple-Output (mMIMO) technology has been implemented to concurrently address multiple devices at the same frequency from a single base station. Such space-division multiplexing can be combined with spectral multiplexing to enable a very large number of concurrent users, but currently is implemented through computationally intensive digital beamforming networks. We show that a radio-frequency (RF) photonic receiver system, previously shown to be capable of sorting signals into respective spatial-spectral 'bins' is further capable, through an injection-locked tunable optical local oscillator (TOLO), of recovering the data upon each signal in the RF scene. The TOLO is combined in free-space with an up-converted optical sideband and the combined optical field impinges upon an array of photodetectors, each corresponding to separate points in k-space, defined by unique combinations of angle-of-arrival (AoA) and carrier frequency. Using this free-space LO insertion, we demonstrate simultaneous recovery of multiple spatially co-located data streams with resilience to interference.**

***Index Terms*—Radio-frequency (RF) photonics, spatial-spectral imaging, signal recovery, down-conversion, quadrature amplitude modulation (QAM), fifth-generation communication (5G), jamming.**

I. Introduction

MOBILE subscriptions have eclipsed the global population and are projected to continue increasing at a linear rate for at least the next five years [1] with the rise of fifth-generation wireless technology (5G). The use of various multiple-access techniques such as code-division multiple access (CDMA), time-division multiple access (TDMA), frequency-division multiple access (FDMA), space-division multiple access (SDMA), and others have given rise to the fertile study of digital beamforming and array processing using the multiple-input multiple-output (MIMO) paradigm. When there exist multiple end users in the space addressed by the base station, this paradigm is referred to as multiple-user MIMO (MU-MIMO). Concurrently addressing many users is typically implemented by a array of transceiving antennas ("base station") using channel state estimation to identify the 'best' path from the base station to each end user in the field [2]–[5]. Modern digital beamforming techniques analyze the data stream from the array in the digital domain, recording the received signal from each antenna and diagonalizing the so-called channel matrix, of size $M \times N$, for M transmitters or sources and N antennas [6]. More recently, 'massive' MIMO systems have been introduced with orders of magnitude higher antenna counts, allowing the base station to perform more complex beamforming [7]. However, the computational complexity of the digital beamforming process increases rapidly for large M or N regardless of the multiple-access technique used; performing spatial de-multiplexing typically relies upon a Fourier transform of the input field; for N antennas the complexity of the fast Fourier transform (FFT) scales as $M \log(M)$. Further, using a channel inversion algorithm such as BLAST (or V-BLAST) can scale at up to NM^3 [8]. The use of 'training' or 'pilot' signals to determine the channel-state information (CSI) is necessary to reap the benefit of MU-MIMO; without accounting for multipath effects and using the beamforming capability of the base station the additional benefit of an arrayed base station is lost [9], [10]

The aforementioned scaling issues are undoubtedly compounded with next-generation wireless networks, as 5G and proposed beyond 5G (B5G) wireless network standards contain provisions for ad-hoc networking and ultra-high user density [11]. In addition, as carrier frequencies increase into the millimeter-wave (mmW) spectrum, hardware for digital beamforming becomes prohibitively expensive, in cases where it exists at all. However, by up-converting the incident RF field to an optical carrier, an RF-photonic imaging system may alleviate the computational complexity for spatial beamforming through the use of a lens to directly take an analog Fourier transform of an optically up-converted representation of the input RF field. Such systems require only the use of a comparitively low-speed phase-locked loop (PLL) to align the phases of the optical carriers, upon which sidebands corresponding to the incident RF field have been created through phase modulators. An abstract representation of this 'hybrid' system layout is shown in Figure 1 in which RF signals are shown in orange, optical signals are shown in blue, and digital control signals are shown in green. This architecture has been extensively demonstrated to be capable of performing spatial multiplexing and cueing detection in a variety of environments with a range of operating bandwidths, antenna counts, and spatial resolution [12]–[15]. This architecture has also been shown to be capable of signal

Manuscript received May 30, 2021; revised September 10, 2021; accepted September 27, 2021. Date of publication September 29, 2021; date of current version January 16, 2022. This work was supported by the Air Force Research Laboratory under Grant FA8750-18-C-0182. *(Corresponding author: William L. Beardell.)*

William Beardell, Conor Ryan, Garrett Schneider, Janusz Murakowski, and Dennis Prather are with the University of Delaware Department of Electrical and Computer Engineering, Newark, DE 19716 USA (e-mail: beardell@udel.edu; cjryan@udel.edu; gschneid@UDel.Edu; jam@udel.edu; dprather@udel.edu).

Benjamin Mazur is with the Phase Sensitive Innovations, Inc., Newark, DE 19713 USA (e-mail: mazur@phasesensitiveinc.com).

Color versions of one or more figures in this article are available at https://doi.org/10.1109/JLT.2021.3116527.

Digital Object Identifier 10.1109/JLT.2021.3116527

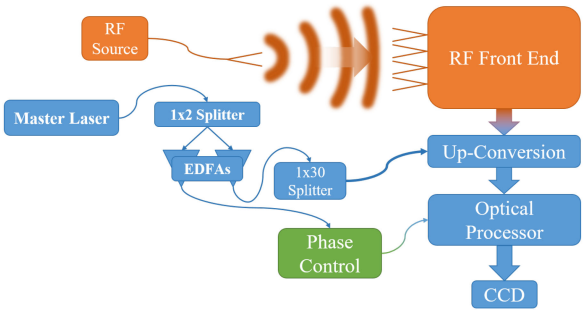

Fig. 1. Flow chart outlining signal paths through distributed aperture millimeter-wave imaging system. RF signals and devices in orange, optical signals and devices in blue, and electronic (digital) signals in green, for phase-locked loop enabling coherent summation of input field at charge-coupled device (CCD) camera. EDFA = Erbium doped fiber amplifier(s) used to amplify master laser signal for use in coherent up-conversion and phase-locked loop.

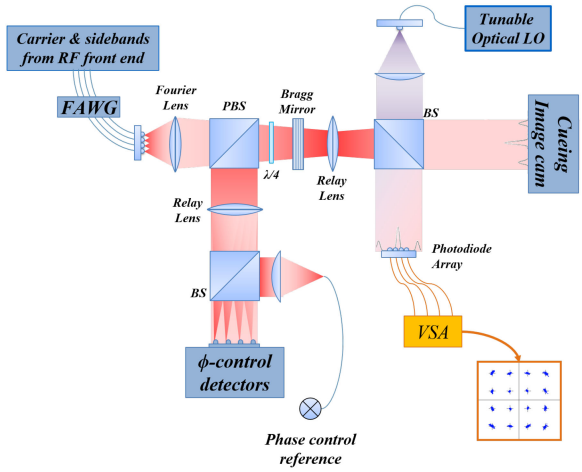

Fig. 2. Notional optical processor layout for phase-locked imaging system, including signal recovery capability. Tunable Optical Local Oscillator (TOLO) injected into free-space and overlaid upon optical sidebands carrying incident RF energy creates a beat signal at a desired intermediate frequency (IF) which is picked up by the photodiode array and read by vector signal analyzer (VSA).

recovery through the use of a tunable optically-paired source (TOPS) for heterodyne down-conversion of the previously up-converted RF signals [16], [17].

More recently, this hybrid RF imaging platform has been updated to include a dispersive characteristic, enabling algorithmic [18], [19] and later direct [20] identification of spectral locations of sources in the RF 'scene' addressed by the antenna array. Such 'cueing' detection allows for rapid identification of channel-state information for all sources within the spatial-spectral field-of-view (FOV), which is determined by system characteristics such as antenna spacing, amplifier bandwidth, path length differences, and other design parameters. While previously published work has demonstrated the capability of a fiber-based arrayed waveguide grating (FAWG) in this application to introduce spectral dispersion at the image plane of the Fourier optical processor for the purpose of cueing detection [20], in this paper we demonstrate the capability of the spatial-spectral channelizing imager to additionally perform signal recovery. This capability is enabled through the use of a tunable optical local oscillator (TOLO) which is injection locked to a modulation sideband of the 'master' laser supplying the array of up-conversion modules. This optically paired source [21] is capable of rapidly changing its offset from the master over an extremely broad bandwidth, allowing for fast adaptation to changing source characteristics, which can be identified through the spectral dispersion of the FAWG.

We show in this work that the presented system configuration is capable of simultaneously recovering at least two data streams broadcast from the same physical location on different carriers, is resistant to co-located interference, and shows strong rejection of unwanted signal in the received band of the desired data stream. In Section II, we outline the general layout of the system from the antenna array through to the image plane of the optical processor. In Section III, we discuss the spatial-spectral channelization performed by the FAWG and free-space optics. In Section IV, we discuss the TOLO used for IF down-conversion. Experimental results for a variety of test cases are presented and discussed in Section V. Finally, a summary of findings and conclusion are presented in Section VI.

II. System Configuration

A. Overview

The overall system topology used for the duration of this work is fundamentally similar to that discussed in [13], [15] and includes the fiber arrayed waveguide grating (FAWG) discussed in [20]. A diagram of the optical processor used in the spatial-spectral RF imager is shown in Figure 2, which includes the free-space insertion of the TOLO, as will be discussed later. A laser source is fed into an optical fiber network allowing for the simultaneous distribution of the carrier to 30 up-conversion modules, each consisting of a linear tapered slot antenna (LTSA) followed by a low-noise amplifier (LNA) serving as the signal input into a phase modulator. This RF front-end is designed for operation in the Ka-band, hence each component in this chain has been selected for operation within the 26.5 to 40 GHz spectral range.

A patented technique [22] allows the distributed antenna aperture to coherently up-convert an incident RF field to the optical domain for passive beam-space processing. This preservation of an incident phase front through the up-conversion process enables beam-space processing of the incident field using free-space interferometry of optical beams [23], [24]. A series of bi-convex lenses take the Fourier transform of the optical field at the input of the free-space optics ("Optical Processor") while distributed Bragg reflector (DBR) filters isolate the first lower sideband of the optical signal generated by the phase modulation of the incident light, while the rejected optical carriers are used to maintain spatial coherence among the array elements as described in [22]–[24]

B. Optical Processor

The optical imaging of the source distribution ("RF scene") impinging upon the antenna array is enabled by the use of an optical array representing a scaled version of the antenna array.

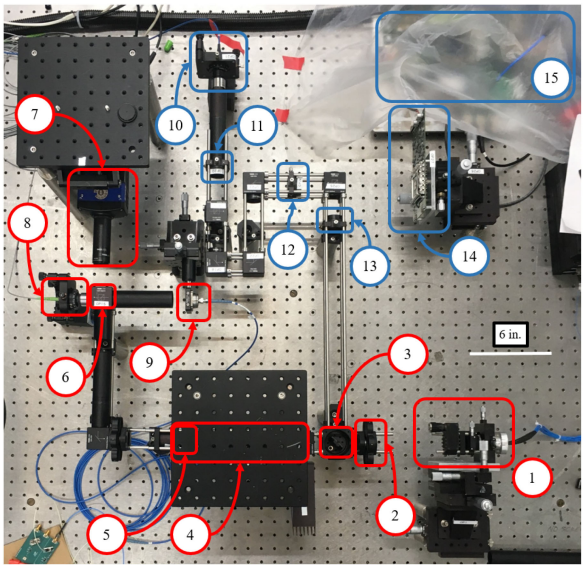

Fig. 3. Configuration of free-space optical processor. 1: Fiber bundle and microlens assembly. 2: Fourier Transform lens. 3: Beam splitter. 4: Dielectric Bragg Grating filters. 5: Image relay lens. 6: Beam splitter/combiner for heterodyne injection. 7: Charge-coupled device (CCD) camera for image readout. 8: Optical LO free-space injection. 9: Photodiode pickup location. 10-14: Phase-locking components and detection board. 15: Field-Programmable Gate Array (FPGA) control board.

Through coherent up-conversion, the optical phase front at the front focal plane of the primary imaging lens is a correspondingly scaled version of the RF phase front. A given combination of frequency and angle-of-arrival (AoA) for a plane wave represents a unique point in **k**-space. For a two-dimensional distribution of antennas, introducing variations in fiber lengths from the antenna array to the optical array creates a dispersive characteristic, allowing for the ability to concurrently identify the full channel-state information (CSI) for each source in the RF scene [18], [19].

In the optical processor configuration shown in Figure 3, the first optical element encountered after the fiber bundle and microlens array assembly (1) is the primary lens of the system (2), which performs a Fourier transform of the optical field at the waist location of the microlens array. Following propagation through the Fourier lens, the optical beams pass through the beam-splitter (3) before reaching the distributed Bragg reflector (DBR) mirrors (4) used for carrier rejection at the image plane. The filters are placed around the back focal plane of the Fourier transform lens so the diameter of the total optical field is as narrow as possible, providing the most uniform response. The reflected carrier energy from the filter step is then returned through the beam-splitter and used to align the phase of each channel for coherent optical imaging of the RF scene [23].

Following the carrier removal stage, a second lens (5) relays an image of the Fourier transform to the camera (7). In the typical configuration, this second lens is positioned such that the Fourier plane of the primary lens is two focal lengths in front of the relay lens, which puts the image plane two focal lengths behind the relay with no magnification. Overall, if the primary and secondary lenses are the same strength, the imaging path is six focal lengths long, and is referred to as a 6 f system. Through the use of $f = 125$ mm lenses and fold mirrors, the optical processor fits comfortably on a tabletop as shown in Figure 3. Additionally shown in the Figure are an additional beam-splitter/combiner (6), TOLO insertion point (8), and photodiode pickup (9), used in this experiment for signal recovery.

III. Spatial-Spectral Channelization

While the architecture of both an mmW imager and imaging receiver (without and with signal down-conversion capability, respectively) has previously relied upon the preservation of the incident RF phase front through the up-conversion process, recent developments in so-called **k**-space imaging have instead introduced perturbations to this phase front to generate a dispersive characteristic to the system. In the "tomographic" method discussed in [18], [19], the fiber-to-antenna association for each channel is completely broken to allow for an algorithmic reconstruction of the three-dimensional **k**-space layout of all sources within the scene. This process uniquely identifies each RF source incident upon the antenna array by its angle of arrival (AoA) in the azimuthal and elevation planes while additionally identifying the frequency of the source. Due to the 'scrambled' nature of the phase front, however, direct image acquisition is limited due to the spread interference of all sources across the image plane rather than the diffraction-limited spot convergence of plane waves typically seen in non-dispersive mmW imaging systems. As a result, the signal recovery capability of the tomographic architecture is limited [1] due to the decreased peak power as well as the interference of all sources across the entire detector plane.

Recently, the tomographic method has been supplemented by a fiber arrayed waveguide grating (FAWG) for linear dispersion along one axis of the array. Through the steering of the RF phase front by a known value that scales with RF source frequency, the nearly instantaneous sorting of signals into azimuthal angle and frequency bins, without the computational latency of tomographic approaches, has been demonstrated [20]. The primary benefit of this configuration is the preservation of coherence within the RF phase front, resulting in a point-spread function (PSF) with a sharp maximum that is linearly translated across the image plane by variations in source AoA and frequency. Further, for cases of multiple sources in the scene, simultaneous, zero-computation separation of the signals is obtained thanks to the strong confinement of optical energy within the main lobe of each PSF and the linear nature of the system. In sum, provided all sources are held to a fixed and common elevation angle, there exists a direct relationship between a spot's vertical location (in v on the image plane as shown in Figure 4) and the carrier frequency of the corresponding source. This relationship is determined exclusively by the FAWG, and enables the fast channelization process novel to this configuration [20]. If a charge-coupled device (CCD) camera is used concurrently with

[1]While the scrambling of phases in the tomographic method results in the spread of energy across the image plane, once cueing detection is performed it is possible to induce a conjugate phase on the antenna array to form a diffraction-limited spot for a single source. However, due to the random nature of the fiber lengths used, this is not possible for multiple sources at the same time.

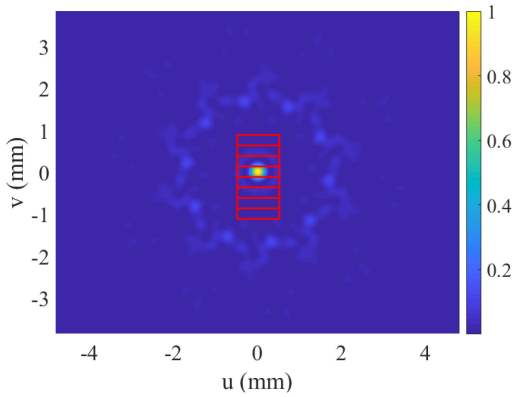

Fig. 4. Normalized simulated PSF for 33 GHz signal with broadside incidence. Photodiode pickup apertures superimposed in red upon PSF to represent element locations at image plane.

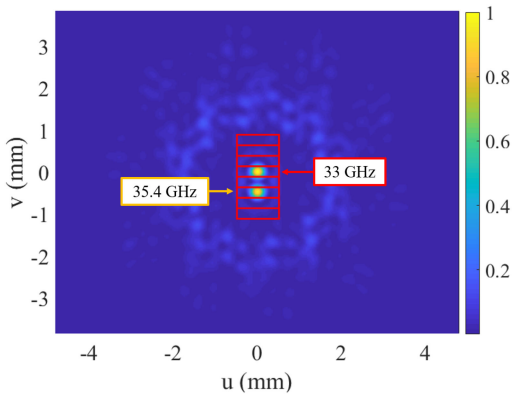

Fig. 5. Normalized simulated PSF showing spatial separation of physically co-located sources displaced in frequency by 2.4 GHz. Signals fall into corresponding photodiodes as indicated by the red superimposed grid.

the signal recovery architecture, the photonic receiver is thus apprised of the carrier frequencies of each source, and is able to reconfigure the tunable optical local oscillator (TOLO) to generate intermediate frequencies (IFs) through down-conversion at the photodiode array.

As discussed in [20], spectral dispersion is introduced into the system response through the use of a FAWG, with fiber lengths linearly dependent upon the vertical position of each antenna in the array. This arrangement induces frequency steering along the vertical axis of the image plane. Due to the linear relationship between the vertical position of the antenna in the array and the optical path length between modulator to fiber bundle, a vertical phase gradient is imposed upon the up-converted RF signal as it passes through the FAWG. To center the main lobe of the PSF on the image plane, a phase offset $\delta\phi_i$ is applied to the i^{th} channel in the array corresponding to the inverse phase change incurred through propagation through the i^{th} channel of the FAWG, modulo 2π [20]. These optical phase offsets compensate, at the design frequency only, for the dispersion phases induced by the true time delays of the unequal fiber lengths. In practice, the phase offsets are determined through a phase calibration procedure and results in a flat optical phase front for a 33 GHz source at broadside to the array [15]. Holding the phase offset for each channel static during system operation results in the acquisition of a frequency- and angle-dependent phase gradient through propagation through the unequal-length fibers, passively steering the beam in the vertical direction on the image plane in proportion to the source carrier frequency.

In the case of all studies presented herein, the design frequency is 33 GHz, such that the center frequency of the operational bandwidth of the imaging system is steered to the center of the image plane. A simulated point-spread function showing a 33-GHz source at broadside incidence is shown in Figure 4. Note the super-imposed array of photodiode pickups — these will be important for the study of signal recovery as discussed in Section V.

As previously discussed, the steering of the main lobe upon the image plane is dependent upon the antenna configuration (for spatial steering) and fiber lengths (for spectral steering). For the

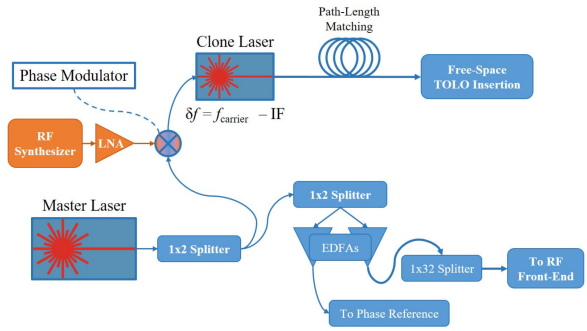

Fig. 6. Block diagram showing Tunable Optical Local Oscillator (TOLO) layout used for IF generation. For free-space down-conversion, recombination onto photodiode does not occur until an RF signal has been modulated onto the 'seed' path as discussed in previous Sections.

current configuration, in which a linear array of photodiodes is placed along the axis of dispersion, a shift in frequency of 1.2 GHz centers the beam upon the adjacent photodetector. This frequency resolution is determined by the longest baseline in the FAWG, or the difference in optical path length between the shortest and longest fibers [20]. This behavior is shown in Figure 5, which shows the simulated response to two sources separated by 2.4 GHz. Note that the signals are separated by two detector grid spacings. The sources are spatially co-located (emanating from the same antenna); this configuration will later be re-created experimentally for verification in Section V-D, Figure 18.

IV. Tunable Optically Paired Source

The optical heterodyne technique used for coherent recovery of incident data signals is of a similar configuration detailed in [16], [17], with the master laser used to feed the optical front end additionally used as the seed laser to injection lock a clone cavity. Before insertion into the clone cavity, the second path of the laser first passes through a phase modulator biased by an overdriven low-noise amplifier, which is in turn fed by a spectrally pure RF synthesizer. This generates an optical comb to which the cavity of the clone laser can be tuned to, and when

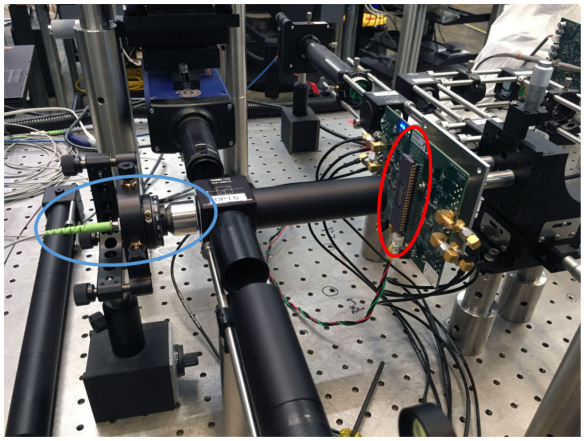

Fig. 7. Detail of optical processor with photodiode array installed. Photodiodes distributed vertically within red oval, corresponding to dispersion axis of FAWG. Optical LO inserted from fiber on left side of image with collimation package outlined in blue. CCD camera in background; optical image of RF scene inserted from bottom of image.

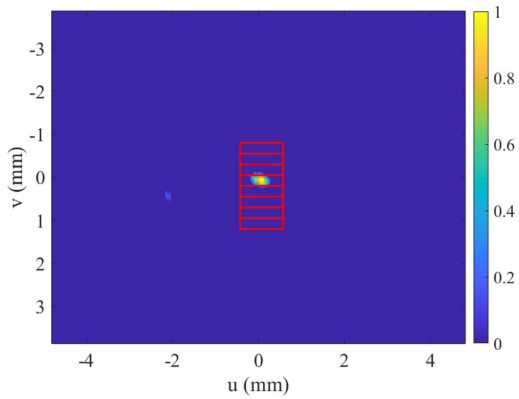

Fig. 8. Normalized experimentally measured PSF for 33 GHz, 5 dBm source signal (with TOLO disabled) and overlaid photodiode pickup positions. Note that pixel values lower than a predetermined threshold return a zero value; in case of main lobe saturation side lobes are visible, as shown in Figure 14.

the two paths are combined the resultant RF tone exhibits high spectral purity due to the correlation of the optical phase noise, provided the path lengths are reasonably matched. This tunable optically paired source (TOPS) configuration is used for ultrawideband signal generation in the absence of an optically-fed RF front-end and has been shown to demonstrate spectrally pure tones from 0.5 to over 110 GHz [21]. With the introduction of an antenna array into the path of the master laser before the two optical signals are recombined, the clone laser may be tuned in concert with the RF synthesizer to create a beat signal at a desired intermediate frequency (IF), with the master laser instead replaced by the modulation sideband generated by the up-conversion modules in the RF front-end. This configuration is defined by the use of the TOPS architecture as a tunable optical local oscillator (TOLO), and enables the recovery of data carried on signals incident upon the array.

The optical feed network for the down-converting mmW imaging receiver is shown in Figure 6. A master laser operating

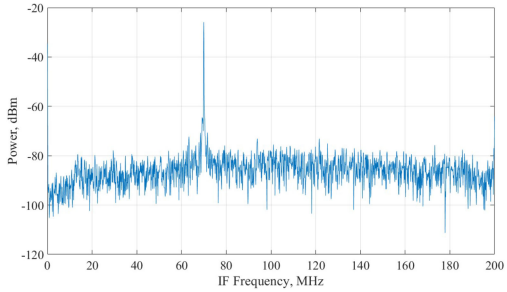

Fig. 9. IF spectrum for single source placed at 33 GHz measured through center photodiode on image plane as shown in Figure 8. TOLO heterodyne signal generated such that IF tone is 70 MHz. IF Power: -26 dBm.

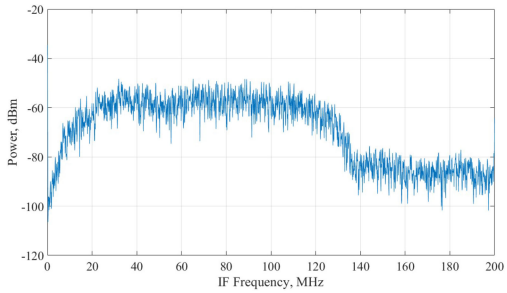

Fig. 10. IF spectrum of 100 MSPS 16-QAM signal. Center frequency 70 MHz, integrated power over signal band -25.39 dBm.

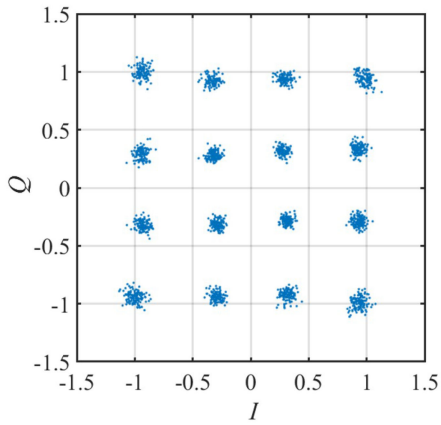

Fig. 11. De-modulated constellation for 100 MSPS 16-QAM signal as measured through center photodiode on Hamamatsu photodiode array. Measured EVM: 6.58% RMS, MER 23.63 dB RMS. In-band IF Power: -25.39 dBm, source power 10 dBm.

at $\lambda = 1557.64$ nm is split two ways, with half of the power directed towards the feed network of the antenna array and the other half directed towards the TOLO componentry. The path taken towards the RF front-end is further split twice and feeds two Erbium Doped Fiber Amplifiers (EDFAs), increasing the optical power for phase locking and imaging. More significant at this juncture, however, is the configuration of the TOLO. As discussed, this optical configuration follows a similar layout to an earlier system, but has been adapted to the present system with the integration of the FAWG. The free-space TOLO insertion

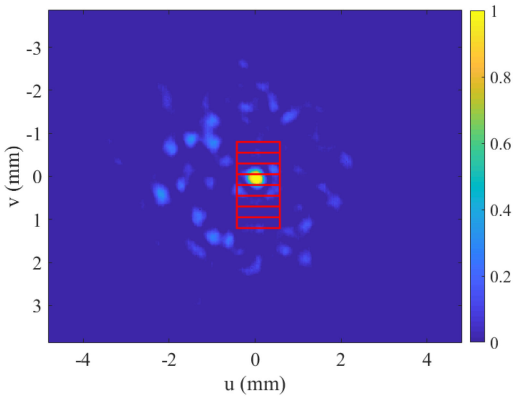

Fig. 12. Normalized experimental PSF for dual incidence of co-located sources with 33 and 33.04 GHz carriers, with no spatial or spectral steering visible at image plane. Moderate side-lobes present in camera response.

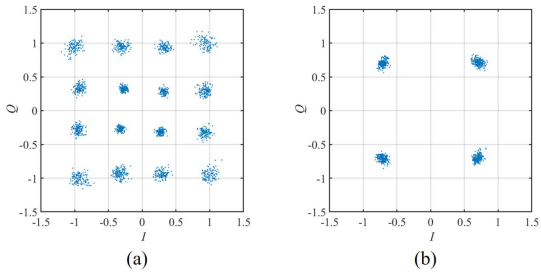

Fig. 13. Recovered constellations for spatially co-located, spectrally adjacent signals. (a): Carrier frequency 33 GHz, IF 40 MHz. EVM: 6.25%, MER 21.45 dB RMS. (b): Carrier frequency: 33.04 GHz, IF 80 MHz. EVM: 6.26%, MER 24.07 dB RMS.

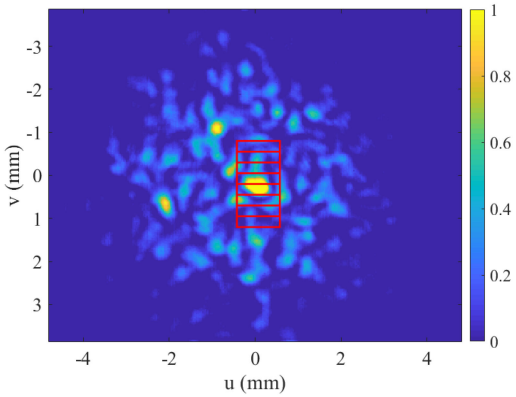

Fig. 14. Normalized Experimental PSF with jamming signal overloading cueing camera. Main lobe from 34 GHz signal combines with 33 GHz signal due to sub-resolution separation. Elevated side-lobe level due to clipping of main lobe and finite dynamic range of CCD Detector.

point corresponds to the block labeled "Tunable Optical LO" in Figure 2 and can be seen in the experimental setup at call-out 8 in Figure 3.

While the TOPS configuration may be tuned by shifting either the master or clone cavity, the DBR mirrors and phase-locking in the optical processor require the master laser wavelength to be

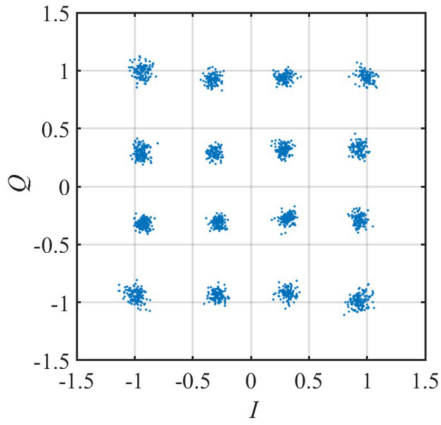

Fig. 15. Recovered constellation for 100 MSPS 16-QAM data signal with 34 GHz, 19 dBm tone propagated through same physical location. Measured EVM: 6.77% RMS, MER 23.39 dB RMS. In-band IF Power: -25.61 dBm, source power 10 dBm.

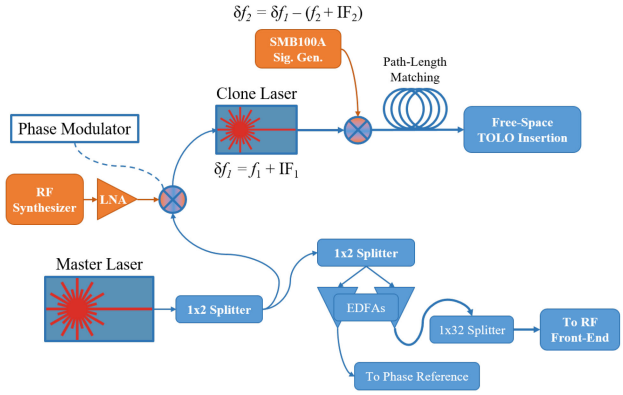

Fig. 16. Flow chart for revised optical configuration enabling simultaneous dual signal recovery. Tone generated by Rohde & Schwarz SMB100 A signal generator corresponds to offset between primary IF and secondary IF, including difference in carrier frequency offset. TOLO is injected into free-space with 'primary' LO tone generated by built-in synthesizer combined with 'secondary' LO tone created by phase modulator overlaid upon entire image plane.

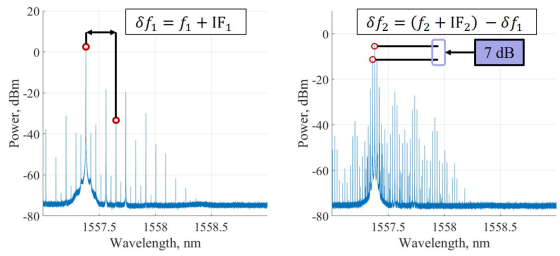

Fig. 17. (a): Optical spectrum at output of TOPS for recovery of a single data stream. Offset δf_1 corresponds to IF of 40 MHz for 33 GHz carrier. (b): Optical spectrum at output of phase modulator used for secondary IF tone generation with $\delta f_2 = 2.45$ GHz continuous-wave phase modulation applied to spectrum shown in (a). With signal generator at maximum power of 13 dBm, amplitude offset between primary and secondary tones measured at 7 dB. Note that 15 dB optical attenuation is applied to both measurements to protect the optical spectrum analyzer (OSA); maximum power measured in (a) was approximately 18 dBm without attenuation.

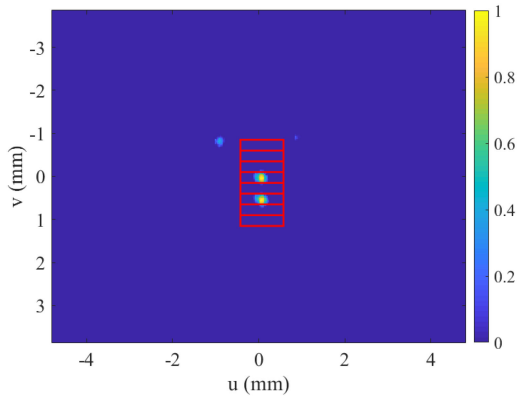

Fig. 18. Experimentally captured point-spread function (with overlaid pickup positions) for dual co-located signal incidence showing spectral separation due to dispersive characteristics of imaging system. Center spot generated by 33 GHz carrier, lower spot generated by 35.4 GHz carrier. Some side lobes present in camera response.

held static in the TOLO configuration. Thus, the RF synthesizer is tuned to create an optical comb with a harmonic at the desired δf, determined by the desired IF for the corresponding carrier. The clone cavity is then tuned to lock to the corresponding harmonic of the optical comb, rejecting the other 'teeth' of the comb. The frequency of the injected seed signal must fall within the injected signal's locking range, determined by both the injection ratio (seeded injection signal to clone laser power) and the frequency difference between the injection seed and the clone laser's free-running oscillations. The output of the clone laser is launched into the optical processor and mixed with the RF sidebands generated by the up-conversion of the RF signal incident upon the array to generate a spectrally pure IF signal suitable for data recovery, tunable over a great deal wider than the Ka-band in which this system is functional.

V. Experimental Results

A. Single-Source Detection

To realize free-space optical down-conversion, a one-dimensional Hamamatsu Photonics photodiode array was integrated into the optical processor. A detail of the pickup configuration is shown in Figure 7. Note that the photodiodes are distributed vertically within the dual in-line package (DIP) inserted into the printed circuit board (PCB) carrying the accompanying bias circuitry and transimpedance amplifiers (TIAs) used to convert the output current from the photodiode package to a voltage signal for use by an electronic signal analyzer (ESA). The entire assembly was then affixed to an *xyz*-translation stage with a one-inch throw along each axis to align the individual photodiodes with the PSF at the image plane. While the PSF is relatively insensitive to minute variations in distance in the axial, or *z,* direction, the pickup surface was positioned at the same distance from the optical beam splitter/combiner as the CCD camera to ensure the overlaid images presented herein represent the correct relative locations of the photodiode array and the PSF.

With the photodiode array installed on the translation stage, a phase calibration was performed [15] to direct the main lobe of the PSF generated from a broadside signal at 33 GHz to the center of the image plane. Following successful calibration, the CCD sensor was covered and the TOLO was enabled. Due to the high power of the TOLO relative to the sideband image power, exposing the CCD sensor to the beam radiated by the TOLO would show a saturated image at best, and at worst could cause damage to the camera. Future optical configurations may be developed to inject the TOLO at a later stage, after the image has been 'tapped' off for cueing detection by the camera for simultaneous cueing and signal recovery.

To align the photodiodes to the pickup plane, the PSF was first observed on the camera to have good confinement of energy to the main lobe with minimal side lobes appearing above threshold on the camera. Due to the band-limited performance of the Hamamatsu Photonics photodiodes, an IF of 70 MHz was chosen. Once the camera was covered and TOLO enabled, the photodiode array was translated on the *(u,v)*-plane to determine the location of maximum power received; this location corresponds to proper alignment of the desired photodiode with the main lobe of the PSF, as shown in Figure 8. For assurance that the TOLO was in the proper place, once the peak power location was determined minor adjustments were made to the TOLO positioning stage to ensure the IF power was at maximum. The experimentally-gathered point-spread function for a 33 GHz source with 5 dBm source power with overlaid photodiode array positions is shown in Figure 8.

The sideband image overlaid with the TOLO signal produces an IF spectrum which is down-converted at the photodetector and measured by the ESA. A WiseWave ARH 2220-02 standard horn antenna with $G_t = 20$ dB of gain was used as a transmit antenna, with signals passed through an RF splitter with 7.2 dB of insertion loss (L_s) and an RF cable with 2.82 dB of insertion loss (L_c). The transmit horn antenna was placed a distance R of 4 meters from the array. With this configuration, a 33 GHz 10 dBm source mixes down to a CW tone at an intermediate frequency of 70 MHz with RF power of -26 dBm. The IF spectrum as measured by the ESA is shown in Figure 9. Using the Friis transmission equation

$$P_a = P_t - L_s - L_c + G_t + 20 * \log \frac{1}{4\pi R}, \qquad (1)$$

the RF power at the antenna array P_a is -14 dBm, indicating the system losses due to RF and optical array efficiency, up- and down-conversion efficiency, free-space loss in the optical processor, and fiber facet loss have a combined value of 12 dB greater than gains afforded by RF and optical array design, low-noise amplifier gain, and added power from the optical carrier.

Verification of the signal recovery capability in this configuration was performed with a 16-QAM signal placed on the 33 GHz carrier while the TOLO was spectrally positioned so as to create a suitable IF for read-out by the ESA. To demonstrate the upper bound of system capability a modulation speed of 100 megasymbols per second (MSPS) was used to modulate a 33 GHz carrier. With the TOLO settings held constant from the

previous configuration, the resulting IF is a 100 MHz signal centered on a 70 MHz IF, as shown in Figure 10. The de-modulated constellation is shown in Figure 11; the constellation is recovered with a root-mean-square (RMS) error vector magnitude (EVM) value of 6.58% and an RMS modulation error ratio (MER) of 23.63 dB.

B. Dual Narrowband Signal Recovery

For situations in which the separation of two end users is less than the angular resolution of the RF front-end, frequency division multiplexing is necessary for the base station to be capable of handling dual bit-streams simultaneously. Spectral channels may be assigned to end users at the discretion of the base station, and in general may be distributed anywhere within the overall band of operation. The worst-case scenario is one in which the two physically adjacent data sources have been assigned spectrally adjacent channels. Shown in Figure 12 is an example of such a scenario — two signals with a carrier offset of 40 MHz are emitted from the same antenna, and are indistinguishable at the cueing detector image plane. The 'primary' signal is located at 33 GHz, and carries a data stream represented by a 16-QAM constellation at 30 MSPS. The 'secondary' signal is located at 33.04 GHz, carrying a QPSK data-stream modulated at 20 MSPS.

However, due to the narrow linewidth of the LO beat signal with the sidebands generated by the data sources, both constellations are recovered by the center photodiode in the array. The recovered constellations are shown in Figure 13; the primary signal has EVM of 6.24% and MER of 21.45 dB, while the secondary signal has EVM of 6.26% and MER of 24.07 dB.

C. Jamming Resilience

Due to the band-limited nature of the photodiodes, combined with the dispersive characteristic of the imaging system, the resilience of this signal recovery architecture in the face of a jamming signal is quite strong. To demonstrate this capability, an additional 'jamming' tone was broadcast through the same antenna as the desired data signal at a significantly higher power. Due to the finite dynamic range of the CCD camera, the cueing response is saturated by the jamming signal and rendered useless. An example of such a situation is shown in Figure 14. The jamming signal is a 34 GHz tone, with broadcast power of 19 dBm, the maximum output power available through the Agilent PSG vector signal generator used as a secondary source for this experiment. Both signals are combined using an RF-Lambda RFLT2WDC40 G Y-splitter with 0.3 dB maximum amplitude imbalance and 7.2 dB insertion loss from each arm of the splitter [25]. The primary data source characteristics are returned to the initial configuration, with a carrier frequency of 33 GHz, power of 10 dBm and 16-QAM symbol rate of 100 MSPS.

As shown in Figure 14, having a strong undesired signal co-located with the data stream compromises the ability of the cueing detector to perform channel estimation. However, due to the pre-determined IF generation, the ability of the system to down-convert the desired data stream is unaffected by the jamming signal, as shown in Figure 15. Compared to the single-tone down-conversion EVM and MER values of 6.58% and 23.63 dB, respectively, the EVM and MER values for the 100 MSPS constellation with jamming are 6.77% and 23.39 dB, respectively. Additionally, the in-band IF power was measured at -25.61 dBm, all virtually equivalent values to the single-tone experiment.

D. Dual Wideband Signal Recovery

While IF resilience to jamming is an excellent benefit for the recovery of a single signal from the photodiode corresponding to a known carrier, the single TOLO beam overlaid upon the entire image plane potentially presents a limitation to the ability to recover multiple signals at the same time if the incoming carrier frequencies are distributed over a wide bandwidth. This is due to the band-limited photodiode array, which filters out higher-frequency beat tones generated through the overlay of the TOLO and RF image. To investigate the capability of the system to recover multiple signals at the same time over a larger portion of the operational bandwidth, a revision to the optical configuration was devised in which a secondary LO tone may be injected with a phase modulator onto the primary TOLO and overlaid upon the entire image plane. A flow-chart showing the revised optical configuration is shown in Figure 16.

As shown in Figure 16, the secondary sideband on the TOLO path was generated using a Rohde & Schwarz SMB100 A signal generator with an output frequency equivalent to the difference in carrier frequencies plus IF frequencies desired for both signals. For a primary signal of 33 GHz corresponding to an IF of 40 MHz and secondary signal of 35.4 GHz corresponding to an IF of 90 MHz, the difference in frequency δf_2 is 2.45GHz. Shown in Figure 17(a) is the optical spectrum at the output of the TOLO when set to generate a 40 MHz IF for a 33 GHz carrier. The parameter δf_1 is the frequency offset from the master laser carrier frequency (approximately 193 THz) and the shorter-wavelength sideband generated by the TOLO for IF generation, a value of 33.04 GHz. In Figure 17(b), the additional phase modulator has been enabled and given an RF input of 2.45GHz to generate an additional sideband for combination with the signal at 35.4 GHz. The power offset between the two signals was measured at 7 dB, and is the minimum possible difference in sideband powers for this configuration, with the signal generator set at a maximum power of 13 dBm. A higher signal power could enable better IF power balancing between carrier signals, but this configuration was deemed sufficient to proceed.

Following measurement of the optical spectrum at the output of the TOLO, the revised optical configuration was tested with two RF signals to show the capability of simultaneous recovery of both data streams. The spectral beam-steering was observed to be such that a frequency offset of 1.2 GHz moved the main lobe of the PSF from the center of one photodiode to the center of the adjacent detector. To show the spatial-spectral separation of the channels onto separate photodetectors, it was determined that a frequency offset of double this value would be sufficient. The resulting PSF for two sources radiating from the same antenna is shown in Figure 18.

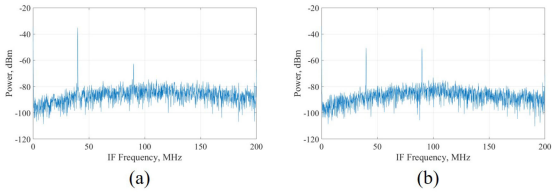

Fig. 19. Measured IF spectra for photodiodes corresponding to 33 GHz (a) and 35.4 GHz (b) RF carriers. 33 GHz carrier mixes down to 40 MHz; 35.4 GHz carrier to 90 MHz. Rejection of undesired signal results from a combination of energy focused towards desired photodiode and difference in LO tone power as discussed previously. Note that power of 40 MHz tone in (b) fluctuates greatly due to increased effect of phase locking fluctuations for sideband energy, while primary 90 MHz tone power fairly constant at -51 dBm.

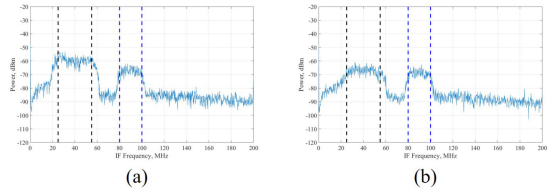

Fig. 20. Measured IF spectra for photodiodes corresponding to the 'primary' 33 GHz (a) and 'secondary' 35.4 GHz (b) carriers. 30 MSPS 16-QAM modulation applied to the primary signal, and 20 MSPS QPSK applied to the secondary. Note attenuation of primary signal in (b) — this is due to a combination of the imbalance in LO power for each frequency as well as the spatial separation of the two signals at the image plane.

As before, the camera must be covered before the TOLO is enabled. When the TOLO is switched on, including the secondary phase modulator and RF bias, the IF spectra measured at the 33 GHz photodiode and 35.4 GHz photodiode shown in Figure 19. Due to the aforementioned 7 dB drop in power for the 'secondary' TOLO sideband used to generate the 90 MHz IF from the 35.4 GHz carrier, the IF power at the corresponding photodiode is less than the IF power measured for the 40 MHz IF at its corresponding detector, despite source powers being equivalent at 10 dBm. The decrease in IF power (-35 dBm versus -25 dBm for previous experiments) for the 'primary' tone is due to the coupling of optical energy in the TOLO from the primary sideband into the secondary sidebands generated by the phase modulator. This effect may be mitigated through the use of an optical amplifier, but an attempt to integrate a semiconductor optical amplifier (SOA) proved to carry too high of a noise penalty to be feasible.

Finally, the ability of this configuration to simultaneously recover two data streams from different carrier frequencies broadcast through the same antenna was measured. Shown in Figure 20 is the IF spectrum presented in a similar manner to that shown in Figure 19 — the spectrum shown in (a) corresponds to that measured at the output of the photodiode intended for the 33 GHz signal, while that shown in (b) corresponds to the 35.4 GHz photodiode.

As before, the signals were de-modulated by the vector signal analyzer in the Rohde & Schwarz FSW for constellation de-modulation and characterization. Shown in Figure 21 are the recovered constellations as measured by the FSW for the

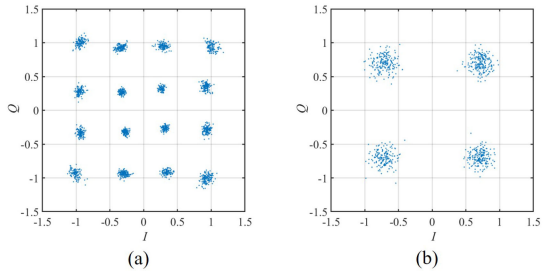

Fig. 21. Recovered constellations at corresponding photodiodes for 33 GHz (a) and 35.4 GHz (b) carriers, each with 30 MSPS 16-QAM signal applied. (a): 5.45% EVM RMS, 27.8 dB MER RMS, (b): 14.35% EVM, 16.86 dB MER RMS.

desired constellations at the corresponding photodetectors; i.e. the 33 GHz signal measured at the center photodiode (a), and the 35.4 GHz signal measured at the second neighbor photodiode (b). As shown in the Figure, the EVM for the 'secondary' tone is increased due to the decreased SNR. However, the capability of this system to separate signals by carrier frequency with gigahertz-order resolution and simultaneously recover multiple data streams from co-located signals over a wide bandwidth has been verified.

VI. Conclusion

In this work, we have shown that a fiber arrayed waveguide grating (FAWG) implemented on the back-end of an optical phased array is able to not only multiplex signals of an arbitrary spatial-spectral distribution, but recover the data stream on each signal in the field of view with the use of a tunable optical local oscillator (TOLO) and an array of photodiodes. The fidelity of the TOLO enables concurrent down-conversion of spectrally close sources regardless of spatial separation, and the system architecture with minor revisions is capable of recovering multiple signals over a very large bandwidth. This wide-band performance is currently limited by the TOPS injection, in which the optical LO is overlaid upon the entire image plane. In order to achieve full separation of sources at the IF, the TOPS signal may be injected with a collimation package overlaying an optical LO onto each photodiode. A notional system with this capability would consist of multiple TOLO signals injected into free-space through a fiber v-groove array followed by a microlens array, confining the light from each fiber into a strongly focused beam in a manner similar to that used for the launch plane of the fiber array carrying the RF image. With such a configuration, cross-talk at the pickup plane would be entirely limited by the confinement of the TOLO beam due to the band-limited nature of the photodiodes; down-conversion of non-corresponding spectral tones would be very far out of band at the desired IF for each detector. In a practical application, the maximization of signal-to-noise ratio (SNR) for the highest number of sources is of unmistakable importance. While the CCD camera has a pixel pitch of 30 microns, the photodiode pitch and spot size of 250 microns greatly discretizes the image plane in the context of signal recovery. A system of this architecture constructed for

operation in an RF-photonic link would therefore require a level of adaptibility to maximize the received power for beams which, in general, do not fall precisely within the active area of the photodiodes. However, the ability of the presented architecture to instantaneously detect the spatial-spectral locations of signals means that the phase front across the array generated by each source is known based upon the spot location on the image plane. If a CCD is used concurrently with the photodiode array, point-spread function engineering may be performed to steer the front-end phases in a calculable manner to maximize spot overlay with photodetectors for the highest number of sources [26].

ACKNOWLEDGMENT

The authors would like to thank the Air Force Research Laboratory for supporting this work.

REFERENCES

[1] P. Cerwall, P. Jonsson, R. Mller, S. Bävertoft, S. Carson, and I. Godor, , "Ericsson mobility report," Ericsson AB, Stochkolm, Sweden, Tech. Rep. EAB-20:009174, Nov. 2020.

[2] H. Dai and H. V. Poor, "Iterative space-time processing for multiuser detection in multipath CDMA channels," *IEEE Trans. Signal Process.*, vol. 50, no. 9, pp. 2116–2127, Sep. 2002.

[3] E. Biglieri *et al.*, *MIMO Wireless Communications.* Cambridge, U.K.: Cambridge Univ. Press, 2007, Chap. 6.

[4] S. Coleri, M. Ergen, A. Puri, and A. Bahai, "Channel estimation techniques based on pilot arrangement in OFDM systems," *IEEE Trans. Broadcast.*, vol. 48, no. 3, pp. 223–229, Sep. 2002.

[5] H. Chaouech and R. Bouallegue, "Multiuser detection and channel estimation for multibeam satellite communications," *Int. J. Comput. Netw. Commun.*, vol. 4, no. 1, pp. 163–174, Jan. 2012.

[6] A. Ghosh *et al.*, *Fundamentals of LTE*. Upper Saddle River, NJ, USA: Prentice Hall, 2011, Chap. 5.

[7] L. Lu, G. Y. Li, A. L. Swindlehurst, A. Ashikhmin, and R. Zhang, "An overview of massive MIMO: Benefits and challenges," *IEEE J. Sel. Topics Signal Process.*, vol. 8, no. 5, pp. 742–758, Oct. 2014.

[8] J. Benesty, Y. Huang, and J. Chen, "A fast recursive algorithm for optimum sequential signal detection in a BLAST system," *IEEE Trans. Signal Process.*, vol. 51, no. 7, pp. 1722–1730, Jul. 2003.

[9] G. Caire, N. Jindal, M. Kobayashi, and N. Ravindran, "Multiuser MIMO achievable rates with downlink training and channel state feedback," Nov. 2007, *arXiv:0711.2642v1* [*cs.IT*], doi: 10.1109/TIT.2010.2046225.

[10] G. Caire and S. Shamai, "On the achievable throughput of a multiantenna gaussian broadcast channel," *IEEE Trans. Inf. Theory*, vol. 49, no. 7, pp. 1691–1706, Jul. 2003.

[11] 5G Americas, "Mobile communications beyond 2020 the evolution of 5G towards next G," White Paper, 5G Americas, 2020.

[12] R. D. Martin *et al.*, "Video rate passive millimeter-wave imager utilizing optical upconversion with improved size, weight, and power," in *Proc. SPIE*, vol. 9462, 2015, Art. no. 946209.

[13] R. Martin *et al.*, "Design and performance of a distributed aperture millimeter-wave imaging system using optical upconversion," in *Proc. SPIE*, vol. 7309, 2009, Art. no. 730908.

[14] D. Mackrides *et al.*, "Progress toward a video-rate, passive millimeter-wave imager for brownout mitigation," in *Proc. SPIE*, vol. 8022, 2011, Art. no. 802203.

[15] C. Schuetz *et al.*, "Realization of a video-rate distributed aperture millimeter-wave imaging system using optical upconversion," in *Proc. SPIE*, vol. 8715, 2013, Art. no. 87150I.

[16] J. Deroba, G. J. Schneider, C. A. Schuetz, and D. W. Prather, "Multifunction radio frequency photonic array with beam-space down-converting receiver," *IEEE Trans. Aerosp. Electron. Syst.*, vol. 54, no. 6, pp. 2746–2761, Dec. 2018.

[17] D. W. Prather *et al.*, "Optically upconverted, spatially cohrent phased-array-antenna feed networks for beam-space MIMO in 5G cellular communications," *IEEE Trans. Antennas Propag.*, vol. 65, no. 12, pp. 6432–6443, Dec. 2017.

[18] J. Murakowski *et al.*, "Photonic probing of radio waves for k-space tomography," *Opt. Exp.*, vol. 25, *no.* 14, 2017.

[19] D. D. Ross, C. J. Ryan, G. J. Schneider, J. Murakowski, and D. W. Prather, "Passive three-dimensional spatial-spectral analysis based on k-space tomography," *IEEE Photon. Technol. Lett.*, vol. 30, no. 9, pp. 817–820, May, 2018.

[20] C. J. Ryan, W. L. Beardell, J. Murakowski, G. J. Schneider, and D. W. Prather, "Instantaneous microwave-photonic spatial-spectral channnelization via k-space imaging," *Opt. Exp.*, vol. 29, no. 13, pp. 19928–19944, Jun. 2021.

[21] G. J. Schneider *et al.*, "Radiofrequency signal-generation system with over seven octaves of continuous tuning," *Nature Photon.*, vol. 7, no. 2, pp. 118–122, Jan. 2013.

[22] R. D. Martin *et al.*, "Controlling the phase of optical carriers," US Patent 8 159 737, Apr. 17, 2012.

[23] T. Dillon *et al.*, "Optical configuration of an upconverted millimeter-wave distributed aperture imaging system," in *Proc. SPIE*, vol. 7485, 2009, Art. no. 74850G.

[24] G. D. Goodno and J. E. Rothenberg, "Engineering of coherently combined, high-power laser systems," A. Brignon Ed. in *Coherent Laser Beam Combining.* Hoboken, NJ, USA: Wiley, 2013, Chap. 1.

[25] RF-Lambda, "Coaxial 1 W 0 2-way power divider DC-40 GHz," RFLT2WDC40G datasheet, *Rev. Aug. 2021*.

[26] J. N. Mait *et al.*, "Millimeter wave imaging with engineered point spread functions," *Opt. Eng.*, vol. 51, no. 9, pp. 1–9, Sep. 2012.